Repowering Steel Tubular Wind Turbine Towers Enhancing them by Internal Stiffening Rings

Yu Hu [1,2], Jian Yang [1,2],* and Charalampos Baniotopoulos [2]

[1]   School of Naval Architecture, Ocean and Civil Engineering, Shanghai Jiao Tong University, Shanghai 200240, China; Y.Hu.6@bham.ac.uk

[2]   School of Civil Engineering, University of Birmingham, Edgbaston, Birmingham B15 2TT, UK; c.baniotopoulos@bham.ac.uk

*   Correspondence: j.yang.1@sjtu.edu.cn

Abstract: This paper presents a robust repowering approach to the structural response of tubular steel wind turbine towers enhanced by internal stiffening rings. First, a structural response simulation model was validated by comparison with the existing experimental data. This was then followed with a mesh density sensitivity analysis to obtain the optimum element size. When the outdated wind turbine system needs to be upgraded, the wall thickness, the mid-section width-to-thickness ratio and the spacing of the stiffening rings of wind turbine tower were considered as the critical design variables for repowering. The efficiency repowering range of these design variables of wind turbine towers of various heights between 50 and 250 m can be provided through the numerical analysis. Finally, the results of efficiency repowering range of design variables can be used to propose a new optimum design of the wind turbine system when repowering a wind farm.

Keywords: wind turbine tower; shell structure; finite element analysis; stiffening ring; sensitivity analysis; repowering

1. Introduction

Due to the growing awareness of environmental protection, wind energy has been extensively used in order to meet the renewable energy production targets in the past 30 years. Therefore, the wind energy technology has been rapidly evolving from small size wind turbines at the kilowatt level rated power to large size wind turbines at the megawatt level rated power. On average, an effective lifetime of a wind turbine could last 20 years but could be extended to 25 years by performing some lifetime extension policies. Therefore, the wind turbine technology in a wind farm could be outdated in half of the lifetime of the wind farm. Furthermore, as the wind farms in better wind condition are usually exploited in earlier time, some wind resources in older wind farms are not completely utilized to generate electricity since older wind turbine installations relatively imply lower power capacity. Therefore, novel technology use in the wind energy system has dramatically grown the power output of new turbines comparing with the old ones [1].

When some wind farms are close to the end of its lifetime, an aging fleet could occur in the wind farm. Then, there are several options to be considered by its wind turbine operators: dismantling the turbine, embarking on a lifetime extension or repowering [2]. Repowering is the process of replacing older wind turbines with newer ones and of using the same place with the output capacity of power in the wind farm increases. By repowering old wind turbines with new upgrades, the increased size and efficiency of the new turbines will increase the amount of energy from a given wind farm. The repowering can happen in two different approaches involving partial repowering and full repowering. Partial repowering is as small as upgrading the main old components, particularly

the rotor and gearbox with new ones whereas retaining other elements such as the foundation and tower. For full repowering, it means that the entire wind turbine systems including the towers and foundations are updated by new units to obtain higher energy efficiency. The repowering of wind farms can keep the wind power plant running and save the total investment costs, as some of the decommissioning and installation expenses can be shared and the wind resource is well known to lower the risk of the project. With less costs and a higher energy output, the repowering process is excessively beneficial. Wind turbines, being the principal technology for the generation of electrical power as wind energy converters, have been extensively investigated with respect to their capacity, effectiveness and safety. A large collection of research results has been accumulated with reference to the structural response of wind energy converters. For instance, Tziavos et al. [3,4] performed the structural performance of grouted connections under large moments by using a nonlinear finite element analysis. Li et al. [5] analyzed the reasons for wind turbine tower collapse under extreme wind loads, and they proposed a robust design for wind turbine towers against typhoons. Kilic et al. [6] measured and predicted the behavior of wind turbine towers by using wireless sensor networks and accelerometers. Binh et al. [7] proposed evaluation formulas for the design wind load on the supporting structure in complex terrains, and these formulas have been validated by comparing analytical solutions with the respective finite element model simulations. Kim et al. [8] carried out seismic analysis of offshore wind turbine towers by considering the soil–pile interaction. The critical displacement was obtained to assess the structural safety under seismic loads by using pushover analysis. Tondini et al. [9] reported the structural response of high strength steel circular columns subjected to fire loading by comparing numerical and experimental results. Van der Woude et al. [10] performed parametric studies on base isolation systems to improve the structural response of wind turbine structures during strong earthquake events; it was concluded that the use of base isolation systems reduces possible excessive dynamic displacements of the structures in seismic zones. Tran et al. [11] described the influence of the door opening on the strength of wind turbine towers by means of detailed finite element models. Do et al. [12] studied the structural response of towers by taking into account fatigue due to wind loads, aiming to minimize the cost of structural steel, and to optimize the design parameters of the tower base and to achieve a longer fatigue life of the towers. Schneider et al. [13] presented the structural response of ring-stiffened cylindrical shells of 50 m height under wind loads using finite element analysis. Valamanesh et al. [14] compared the predicted results with those from a baseline wind turbine tower in operation and at rest, where a reasonable agreement seems to have been achieved. Guo et al. [15] performed a series of bending tests on tower tubes with stiffeners, to investigate the effect of section slenderness on the behavior of the steel tower tubes, and the respective experimental results are in accordance with the AS4100 design code. Ghazijahani et al. [16] considered the effect of an opening on the structural response of a cylindrical shell under axial compression. Sabouri-Ghomi [17] studied the relevant design parameters and in particular, the quantities and dimensions of the stiffening rings with the aim of analyzing their effect on the structural stability of reinforced concrete cooling towers. By using numerical analysis, a method to determine the parameters of the stiffening rings, which could increase the buckling capacity of the cooling towers, was proposed. Perelmuter et al. [18] formulated an optimization problem for the design of steel wind turbine towers by considering the wall thickness, the diameters of the cross-section and the height as design variables. Sim et al. [19] reported a parametric study in which a numerical simulation was compared with experimental results on the flexural buckling strength of a wind turbine tower. Hu et al. [20] studied the effect of varying the number of stiffening rings with respect to wall thickness variation, on the structural response of steel wind turbine towers. Within this framework the most efficient method for selecting the number of stiffening rings and for reducing the wall thickness in order to strengthen the towers and minimize costs was proposed for each height case. Negm et al. [21] chose the cross-sectional area, radius of gyration and height of each segment as design variables, and formulated the design problem as a nonlinear mathematical programming problem. Shi et al. [22] investigated the overall buckling of tubular columns composed of high strength steel by applying experimental testing and numerical simulation,

and the numerical and experimental results were compared with reference to the analytical solutions obtained by applying current code provisions. Zhu et al. [23] studied the optimized mesh size and performed a parametric study of steel oval hollow section columns by using one hundred numerical models. Karpat [24] developed a virtual tool to perform the cost optimization of wind turbine steel towers with rind stiffeners by using the MATLAB procedure, it was found that the variations of the wall thickness and diameter have an important effect on the mass and cost of wind turbine towers. Chen [25] studied the stress and strain distribution of the reinforced concrete beam–slab foundation under various loading states, they thought that a proposed circumferential pressing technique could reduce the tensile stress of concrete on the top surface of the foundation pier. Ding [26] monitored the floating performance of an offshore wind turbine tower with a composite bucket foundation during transportation, they found that the wind turbine could meet the specified acceleration value limits during towing.

To repower a turbine, the wind turbine systems including the tower should be replaced. The higher tower and longer blades can generate more output energy with fewer turbines as higher space has faster and more stable winds. As the tower height is closely related to the energy yield, the appropriate supporting structure for a wind turbine should be designed by taking into account cost effectiveness. To facilitate transportation, wind turbine towers are manufactured in sections that are connected in situ during the erection. Typical tubular steel wind turbine towers are composed of cylindrical or conical shells interconnected by bolted flanges. Obviously, the geometric variation of the stiffening rings greatly affects both the strength and the stability of the towers. To improve the economy in the design of such towers, the wall thickness, the mid-section width-to-thickness ratio and the spacing of the stiffening rings of the wind turbine tower at different height levels should be considered as the critical design variables for repowering to update the old wind farm. Wind turbine tower can be repowered based on the conclusion of the efficiency repowering range of design variables so that the upgradation of wind turbine system in a wind farm can be performed more efficiently. Therefore, the results of efficiency repowering range of design variables can be used to propose a new optimum design of the wind turbine system when repowering a wind farm.

In this paper, a repowering solution with reference to the design of wind turbine towers is numerically performed by means of the finite element software ABAQUS [27]. Firstly, the results of the numerical model are compared with the experimental data obtained by Rebelo et al. [28,29]. Secondly, to repower wind turbine towers in a more efficient way, the wall thickness (referred to as "T"), the mid-section width-to-thickness ratio of the ring sections (referred to as "R") and the spacing of the stiffening rings (referred to as "H") are considered as the repowering design variables for each height case of 50 m, 150 m and 250 m. To obtain a direct comparison, the maximum von Mises stresses and horizontal sways of the finite element model towers are calculated for each height case. Furthermore, the rate of change of the maximum von Mises stresses and of the horizontal sways for three different tower heights with respect to each of the design variables are compared to provide some repowering advices for wind farm by explore the efficiency repowering range of the variables at hand.

2. On the Numerical Modeling

An extensive numerical investigation was performed to study the effect of stiffening rings on the overall response of wind turbine towers. The numerical models were developed using the commercial package ABAQUS. The models were first validated with respect to existing data recently obtained by Rebelo et al. [28,29] who monitored the structural response of an actual wind turbine tower of 76.15 m height.

The tubular cylindrical tower that was monitored was composed of three segments with lengths 21.77 m, 26.62 m and 27.76 m respectively, as shown in Figure 1. The segments are connected to each other by bolted flanges. The mid-section widths of the upper and lower level flanges were 105 mm and 120 mm respectively and the corresponding thicknesses were 120 mm and 175 mm. The diameter varied linearly from 4.3 m at the base to 2.95 m at the top, and the shell thickness decreased linearly

from 30 to 12 mm along its height. The self-weight of the wind turbine was 106.73 t and the turbine was placed at the top of the tower with an eccentricity of 0.72 m. Sensors were fixed at four levels as displayed in Figure 1. Levels 0, 1, 2 and 3 in Figure 1 were located at heights 5.8 m, 17.97 m, 44.59 m and 71.15 m, respectively. In the numerical model, different wall thicknesses were used in four different sections, i.e., 28 mm thickness for heights from 0 to 8.8 m, 22 mm from 8.8 to 21.77 m, 18 mm from 21.77 to 48.39 m and 13 mm from 48.39 to 76.15 m. The tower shell was simulated by the S4R shell element, which is a 4-node doubly curved thin or thick shell element, with a reduced integration finite element with hourglass control, and is capable of considering finite membrane strains. The flanges were simulated by means of the C3D10 continuum finite element, which is a 10-node quadratic tetrahedron element. The interaction between the flange and the tower wall was considered by using tie constraints. The support of the tower was considered as fully fixed. A reference node was introduced with a rigid coupling constraint to the top cross-section of the tower to apply all possible loadings at the top of the tower and was constrained in a kinematic coupling type including six degrees of freedom. The self-weight of the wind turbine, a bending moment created by the gravity of wind turbine with an eccentricity and a horizontal wind load applied on the blades of the towers can be simply applied to the reference node. The horizontal force is 380 kN according to the inventory data of Rebelo et al. [28,29]. A non-linear static analysis has been performed to solve the numerical model. The elastic modulus and the Poisson's ratio of steel were 200 GPa and 0.3 respectively, and the density of steel was 7.85 g/cm^3.
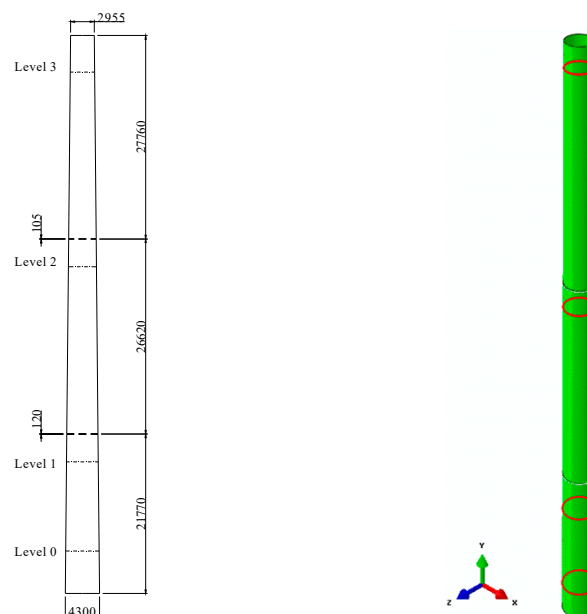

Figure 1. The geometrical data and the finite element model of the wind turbine tower.

Due to the complexity of the load combinations, the wind load profile along the tower height and around the circumference was simulated by using a simplified method: the tower was divided into two parts along the tower height, and separated into four parts around the circumference in accordance with Hu et al. [20], based on BS EN 1991-1-4 [30]. The wind speed was taken at the four levels of the tower, and the maximum wind speed during the testing period was 25 m/s. Wind pressure could be expressed as a function of wind speed by means of the following formula:

$$p = 0.5 \cdot \rho \cdot v^2 \tag{1}$$

where for air density, ρ is equal to 1.25 kg/m^3, for wind speed, v is expressed in m/s, and for the wind pressure, p is in N/m^2.

According to Rebelo et al. [28,29], the magnitude of the average maximum bending moment at the base of the tower under monitoring is 2.9×10^7 N·m. The self-weight of the tower was calculated by the software, based on the dimensions of the tower and the material density.

Since the simulation accuracy and the calculation efficiency of the developed numerical models are affected by the mesh density, a study of the mesh sensitivity is essential (e.g., Lavassas et al. [31], Baniotopoulos et al. [32]). The refined elements may lead to a low efficiency, whereas the rough elements may lead to erroneous results. To obtain the optimum element size for such a tower model, the shell should initially be simulated by means of finite elements of various element sizes. The maximum von Mises stresses and the horizontal sways of the tower under consideration were calculated using models of rough to refined elements, which in turn were examined to attain convergence. The size of the S4R shell element was chosen as between 400 and 50 mm. The size of the C3D10 element of the two flanges was discretized at the size of 50 mm. The maximum von Mises stresses and horizontal sways of the 76.15 m tower structures modeled with different element sizes are presented in Table 1.

Table 1. Maximum von Mises stresses and horizontal sways of the tower for different element sizes.

Size of Elements (mm)	Max. von Mises Stress (MPa)	Max. Horizontal Sway (mm)
400	102.64	575.13
300	103.9	572.8
200	102	570.7
100	101.6	568.5
80	101.6	568.5
50	101.6	568.5

According to the results (Table 1), the maximum von Mises stresses and horizontal sways of this tower were evidently affected by the size of the finite element selected when the element size was reduced from 400 to 100 mm. In Table 1, the maximum von Mises stresses and the horizontal sways of the 76.15 m tower remained almost constant with element sizes reducing from 100 to 50 mm. The maximum von Mises stresses and horizontal sways of the towers converged to 101.6 MPa and 568.5 mm, respectively when the size of the shell elements was reduced to 100 mm. Therefore, the optimum size of the applied S4R shell element of the tower was approximately 100 mm.

As previously mentioned, the tower, which was studied by Rebelo et al. [28,29], was monitored by sensors placed at four different levels. The measured stress at each level was compared with the numerical results of the present model. As wind loading is variable in engineering practice, the stress values should be fluctuating at different wind speeds. Thus, the combination of mean stress value and its standard deviation for each wind speed should be compared with the monitored data to validate the model. According to this data inventory (Rebelo et al. [28,29]), the sum of average vertical stresses and corresponding standard deviation of levels 0 and 1 were respectively 73 MPa and 68 MPa respectively, both being achieved at a wind speed of 12 m/s.

The vertical stress contours at the cross-sections at levels 0 and 1 are depicted in Figure 2. Table 2 shows the comparison errors of numerical and experimental results of the 76.15 m tower. In the cross-section at level 1, the maximum vertical stress was 66.41 MPa, which is close to the measured stress of 68 MPa. Similarly, the maximum stress in the cross-section at level 0 was 72.99 MPa, which was almost identical to the measured stress of 73 MPa at the monitored tower (Figure 2). The measured dynamic horizontal sway of the tower fluctuates. According to Rebelo et al. [28,29], the average maximum horizontal sway of the tower obtained from the experimental monitoring data at level 3 was 534.23 mm. The maximum horizontal sway from the numerical model was 534.8 mm, which was almost identical to the measured average maximum displacement of 534.23 mm as depicted in Figure 3. Thus, a good correlation for maximum vertical stress and horizontal sway between the numerical and the experimental results was achieved according to Table 2.
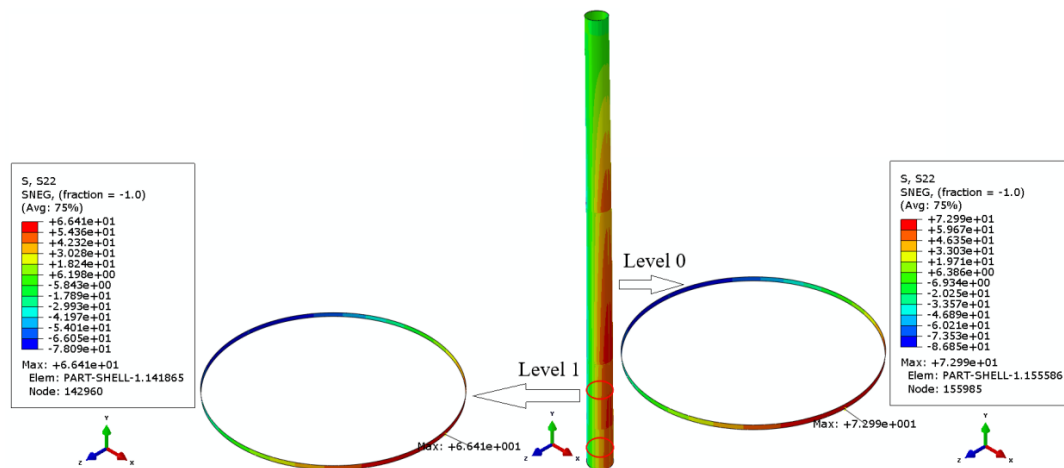
Figure 2. Vertical stress contour plot at the cross-sections of the 76.15 m tower at levels 0 and 1.

Table 2. Comparison of numerical and experimental results of the 76.15 m tower.

Values	Numerical Results	Experimental Results	Errors
Stress at level 0	72.99 MPa	73 MPa	0.01%
Stress at level 1	66.41 MPa	68 MPa	1.96%
Sway at level 3	534.8 mm	534.23 mm	0.1%
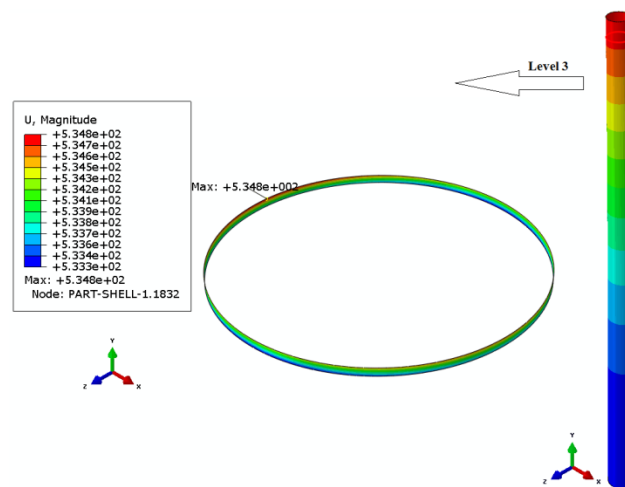
Figure 3. Horizontal sway contour of the cross-section of the 76.15 m tower at level 3.

3. Repowering of Wind Turbine Towers

If a repowering occurs in a wind farm, the old wind turbine system should be dismantled, the tower height should be increased and the wind turbine supporting structures should be also enhanced by internal stiffening rings, therefore, a repowering scheme study including T, R and H was performed for towers, which were 50 m, 150 m and 250 m high. For each height case, a simplified distribution pattern and the magnitude of the wind load along the tower height and around the circumference were considered, as proposed by Hu et al. [20].

3.1. Description of the Wind Turbine Tower Models

3.1.1. The 50 m tower models

The geometrical data and the finite element models of four different distributions of stiffening rings for 50 m towers are presented in Figure 4. The values of H for the 50 m towers were 16.667 m, 10 m, 6.25 m and 4.16 m respectively (referred to as "H_i", "H_{ii}", "H_{iii}" and "H_{iv}" in Figure 4). The diameters reduce linearly from 3.7 m at the base to 2.37 m at the top as shown in Figure 5. The widths of the stiffening rings were 50 mm, 100 mm, 200 mm and 300 mm respectively, and the mid-section thickness of the stiffening rings was 100 mm. Their corresponding values of R are referred to as "R_i", "R_{ii}", "R_{iii}" and "R_{iv}" (Figure 5). Concerning the thickness, four groups of thickness distributions for the 50 m towers are depicted in Table 3. These are, for the lower and upper section, 15/5 mm, 20/10 mm, 25/15 mm and 30/20 mm (referred to as "T_i", "T_{ii}", "T_{iii}" and "T_{iv}"). The corresponding shell weights are also presented in Table 3, and these were 45.49 t, 64.2 t, 82.91 t and 101.62 t. The Young's modulus, the density and the Poisson's ratio of the steel were 205 GPa, 7.85 g/cm^3 and 0.3 respectively.
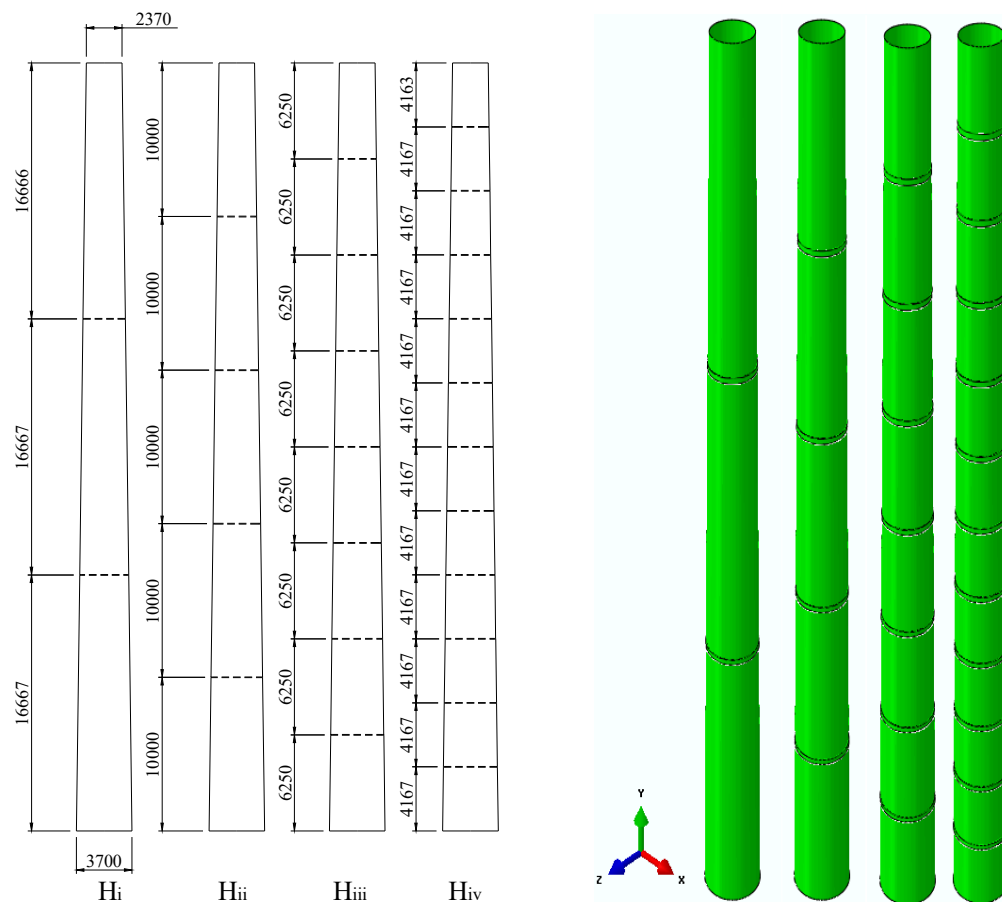

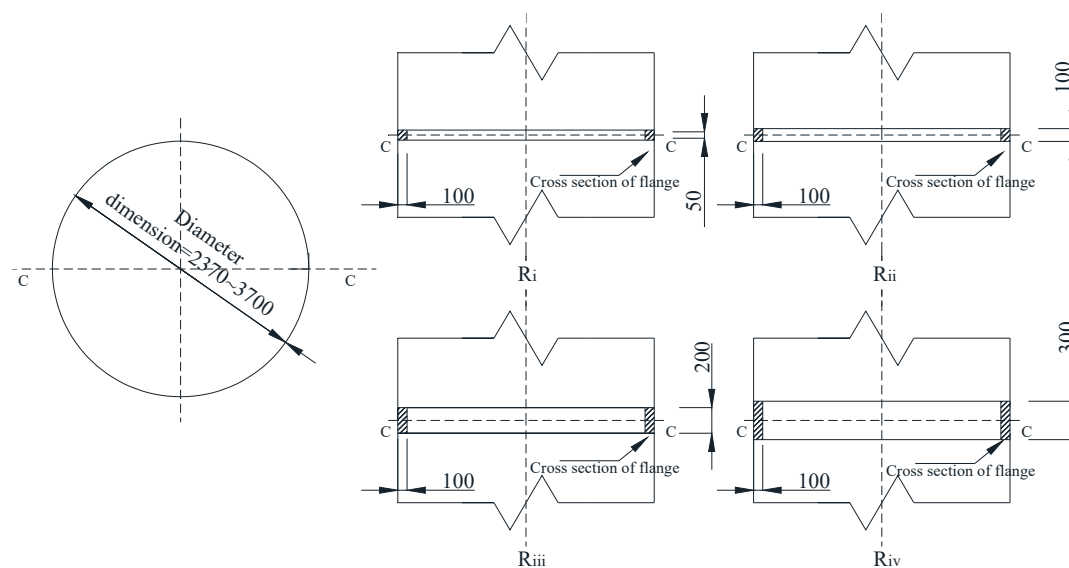**Figure 4.** The 50m-towers: geometrical data and finite element models (in mm).

Figure 5. Typical ring cross-sections of the towers (in mm).

Table 3. Parameter details of the 50 m-towers.

50 m Towers	Height Range of the Towers		Mid-Section Width-to-Thickness Ratio of Rings		Spacing of Rings (m)		Thickness of Rings (mm)
	0–33.334 m Thickness	33.334 m–50 m Thickness					
T_i	15 mm	5 mm	R_i	0.5	H_i	16.667	50
T_{ii}	20 mm	10 mm	R_{ii}	1	H_{ii}	10	100
T_{iii}	25 mm	15 mm	R_{iii}	2	H_{iii}	6.25	200
T_{iv}	30 mm	20 mm	R_{iv}	3	H_{iv}	4.167	300

For the finite element models, the 50 m tower models were composed of S4R shell elements and C3D10 continuum elements, which are the same as those of the 76.15 m tower model. As described in the previous section, the 50 m tower models were discretized by the mesh having a shell element size of 100 mm and a continuum element size of 50 mm. The interaction between the flange and the tower wall was tie constrained, and the base of the tower was considered to be fully fixed. Concerning the loading states for the 50 m towers, the axial, transverse and torsional loads at the top of the tower were applied to a reference node imported with a rigid constraint to the top cross-section of the towers. The magnitudes of the combined loads including wind pressure along the tower height and around the circumference follow the pattern proposed by Hu et al. [20].

The 50 m tower with thickness T_{ii}, mid-section width to a thickness ratio of the stiffening rings R_i, and ring spacing H_i was simplified as $50T_{ii}R_iH_i$, and its contour plots of von Mises stress and horizontal sway are shown in Figure 6. The maximum von Mises stress of $50T_{ii}R_iH_i$ occurred in the inner side of the stiffening ring, and its magnitude was 113.8 MPa, greater than that in the 50 m tower shell, which was 50.89 MPa. The maximum horizontal sway of the 50 m tower was 11.07 mm at the top of the tower as expected (Figure 6).
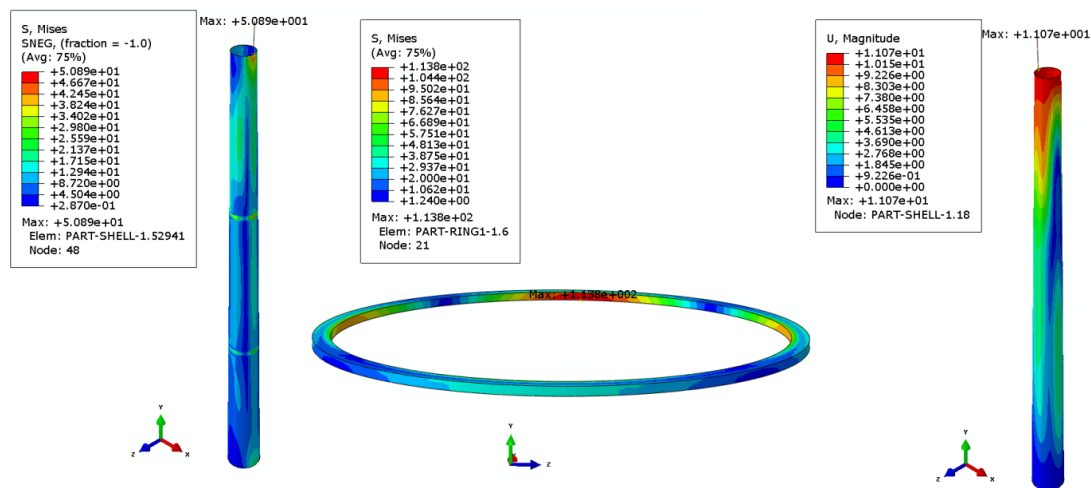
Figure 6. The von Mises stress of the shell and ring and the horizontal sway of the $50T_{ii}R_iH_i$ tower.

3.1.2. The 150 m-Tower Models

The ring spacings, H, for the case of the towers with height 150m are depicted in Figure 7. The ring distances of 18.75 m, 15 m, 11.544 m and 9.375 m are represented as "H_i", "H_{ii}", "H_{iii}" and "H_{iv}" respectively. The dimensions of width and mid-section thickness of the stiffening rings in the 150 m towers were identical to those of the corresponding stiffening rings in the 50 m towers as displayed in Figure 5 (referred to as "R_i", "R_{ii}", "R_{iii}" and "R_{iv}"). For each H, the four groups of wall thicknesses for the 150 m towers were distributed from heights 0 to 50 m, 50 to 100 m and 100 to 150 m. The four groups of thicknesses of the 150 m towers are presented in Table 4 as 40/30/25 mm, 45/35/30 mm, 50/40/35 mm and 55/40/35 mm respectively, (referred to as "T_i", "T_{ii}", "T_{iii}" and "T_{iv}"), and their corresponding weights were 849.01 t, 980.34 t, 1111.67 t and 1242.99 t respectively. The diameters of the cross-sections of the tower wall varied linearly from 8.5 at the base to 5.7 m at the top. The support of the 150 m towers were considered to be fixed, and the types of elements, the material properties and the interaction between the shell and the rings were also similar to those of the 50 m models. The widths of the stiffening rings of the 150 m towers were 50 mm, 100 mm, 200 mm and 300 mm respectively, and the mid-section thickness of the stiffening rings was 100 mm.

Table 4. Parameter details of the 150 m-towers.

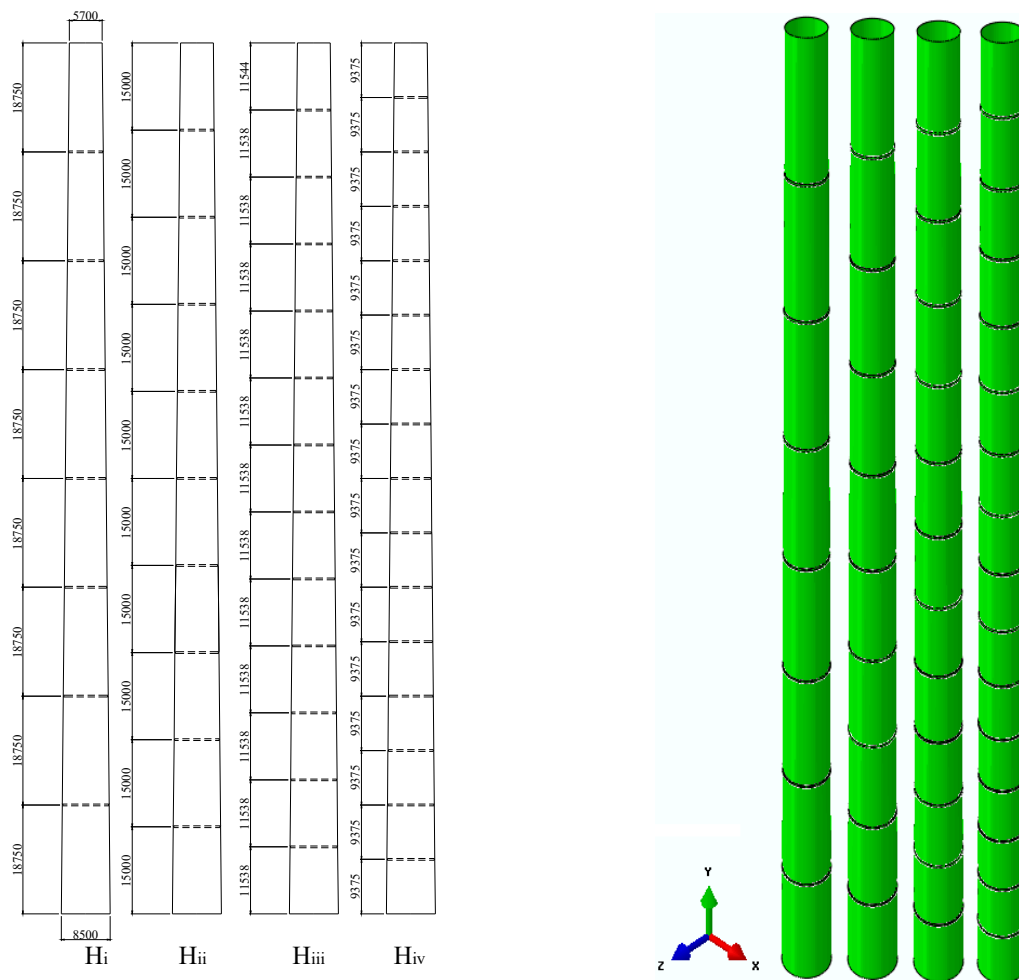| 150 m Towers	Height Range of the Towers			Ratio of Mid-Section Width-to-Thickness of Rings		Spacing of Rings (m)		Thickness of Rings (mm)
	0 to 50 m Thickness	50 to 100 m Thickness	100 to 150 m Thickness					
T_i	40 mm	30 mm	25 mm	R_i	0.5	H_i	18.75	50
T_{ii}	45 mm	35 mm	30 mm	R_{ii}	1	H_{ii}	15	100
T_{iii}	50 mm	40 mm	35 mm	R_{iii}	2	H_{iii}	11.544	200
T_{iv}	55 mm	45 mm	40 mm	R_{iv}	3	H_{iv}	9.375	300

Figure 7. The 150 m-towers: geometrical data and finite element models (in mm).

The maxima for the von Mises stress of the shell and the ring, and the horizontal sway of $150T_{iii}R_iH_i$ are presented in Figure 8. The maximum von Mises stress of the shell was 57.17 MPa and occurred as expected at the base of the tower, whereas the maximum von Mises stress of the stiffening rings was 154.9 MPa, occurring at the inner side of the rings. The horizontal sway increased nonlinearly from 0 at the base to its maximum value of 157.8 mm at the top.
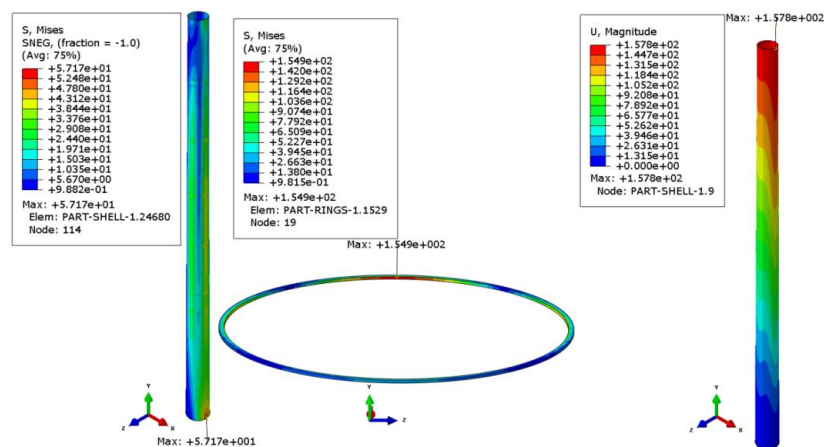

Figure 8. The von Mises stress of shell and ring and the horizontal sway of the $150T_{iii}R_iH_i$ tower.

3.1.3. The 250 m-Tower Models

Four stiffening ring spacing distances for the 250 m towers (2.5 m, 16.667 m, 11.364 m and 8.612 m, referred to as "H_i", "H_{ii}", "H_{iii}" and "H_{iv}" respectively) were investigated, as shown in Figure 9. The four widths of stiffening rings were 50 mm, 100 mm, 200 mm and 300 mm respectively (as shown in Figure 5). The mid-section thickness of all of the stiffening rings of the 250 m-towers was 100 mm. The R of the 250 m towers was 0.5, 1, 2 and 3 respectively (referred to as "R_i", "R_{ii}", "R_{iii}" and "R_{iv}"). The thickness details for the 250 m-towers are presented in Table 5, and the corresponding thickness groups were 60/50/45 mm, 65/55/50 mm, 70/60/55 mm and 75/65/60 mm respectively (referred to as "T_i", "T_{ii}", "T_{iii}" and "T_{iv}"). The diameters of the tubular 250 m towers gradually reduced from 14 to 9.5 m as shown in Figure 9. The base of the 250 m towers was considered as fixed, and the other parameters of the 250 m-tower models were the same as those of the 50 m and 150 m towers.
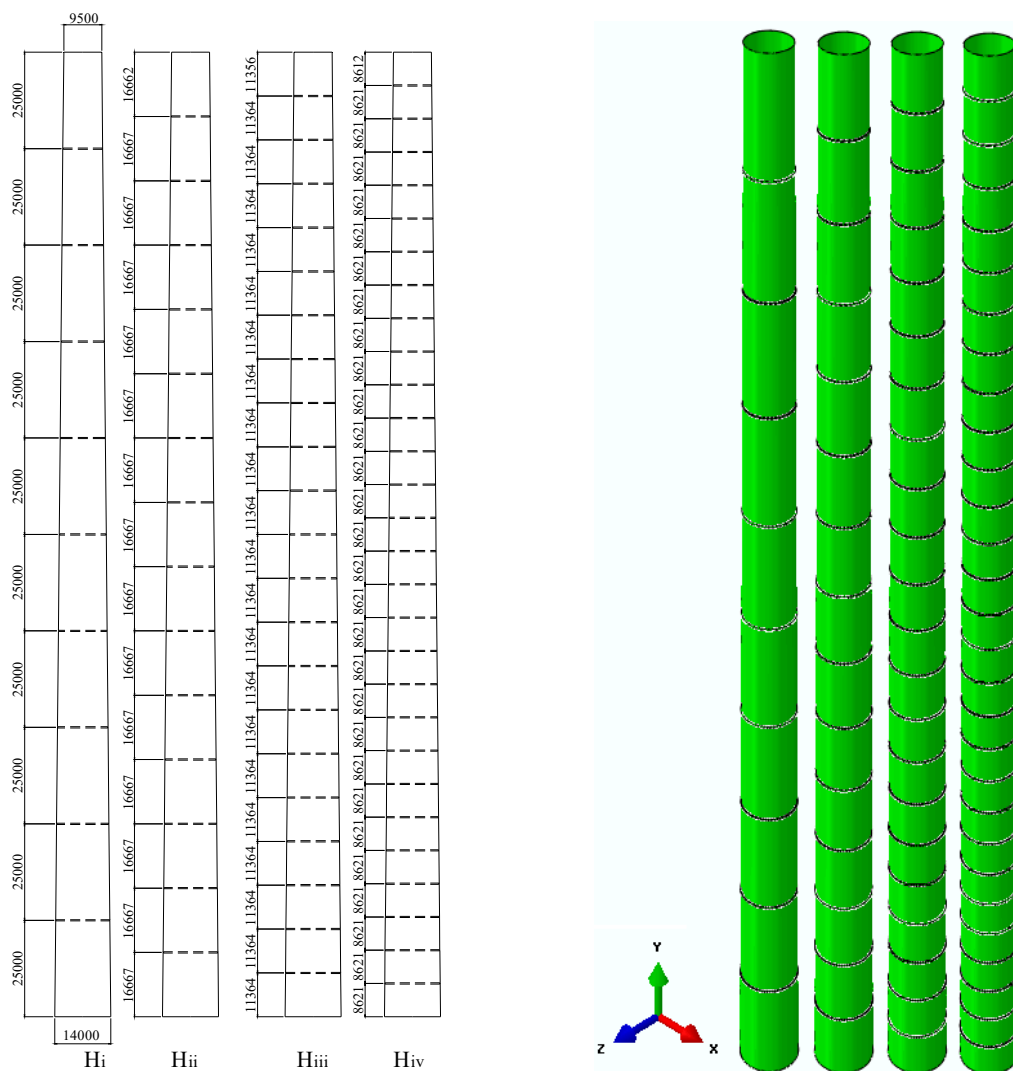

Figure 9. The 250 m-towers: geometrical data and the finite element models (in mm).

Table 5. Parameter details of the 250 m-towers.

250 m Towers	Height Range of the Towers			Ratio of Mid-Section Width-to-Thickness of Rings		Spacing of Rings (m)		Thickness of Rings (mm)
	0 to 100 m Thickness	100 to 200 m Thickness	200 to 250 m Thickness					
T_i	60 mm	50 mm	45 mm	R_i	0.5	H_i	25	50
T_{ii}	65 mm	55 mm	50 mm	R_{ii}	1	H_{ii}	16.667	100
T_{iii}	70 mm	60 mm	65 mm	R_{iii}	2	H_{iii}	11.364	200
T_{iv}	75 mm	65 mm	60 mm	R_{iv}	3	H_{iv}	8.612	300

The contours of the von Mises stress in the shell and in the rings, as well as the horizontal sway of $250T_iR_iH_i$ are displayed in Figure 10. The magnitude of the maximum von Mises stress in the shell was 107.6 MPa, which occurred in the region near the base of the tower. The magnitude of the maximum von Mises stress in the rings was 208.9 MPa, and the maximum horizontal sway was 648.7 mm at the top of the tower.
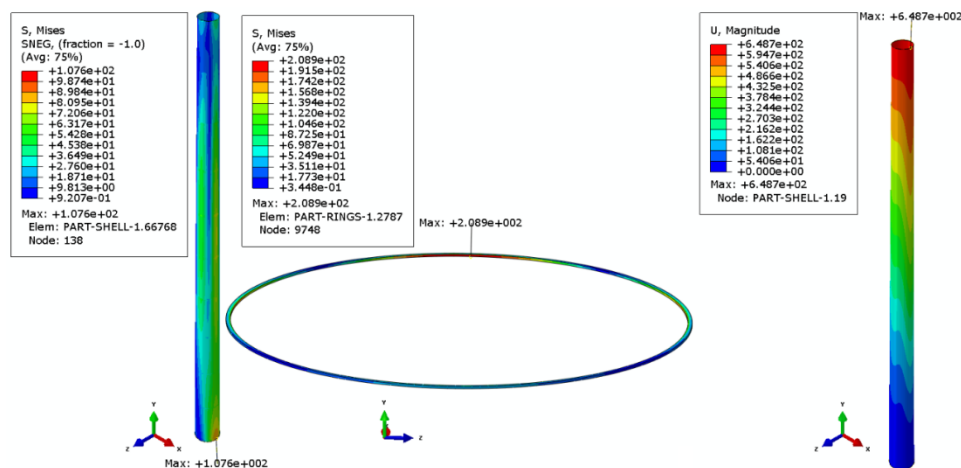

Figure 10. The von Mises stress of the shell and the ring, and the horizontal sway of the $250T_iR_iH_i$ tower.

3.2. Efficiency Repowering Range of Design Variables for Repowering

The wind turbine tower can be repowered based on the results of the efficiency repowering range of the design variables so that the upgradation of wind turbine system in a wind farm can be performed more efficiently. As a more efficient repowering range of design variables of the wind turbine towers at each height level is a better option in cost saving for the strengthening of the towers, the conclusions of efficiency repowering range of the thickness, mid-section width-to-thickness ratio and spacing can be used to propose a new optimum design of the wind turbine system when dismantling a wind farm for repower purpose. In this section, the rate of change of the maximum von Mises stresses and of the horizontal sways for three different tower heights with respect to each of the design variables were compared to provide some repowering advices for wind farm by explore the efficiency repowering range of the variables at hand.

3.2.1. Efficiency Repowering Range of the Thickness T

The maximum von Mises stresses in the tower shell and the maximum horizontal sways of the 50 m towers for each group of thicknesses are presented in Appendix A. For each R and H, the 50 m towers with 15/5 mm, 20/10 mm, 25/15 mm and 30/20 mm thickness were numerically simulated to obtain the maximum von Mises stresses and the horizontal sways (Appendix A). Given that the shell wall thickness was a significant parameter in the design of the tower structure, it was evident that variations in thickness significantly affected the tower's strength and stiffness. Thus, the inherent relationship

between thickness and strength/deflection of the structure was studied, and the efficiency repowering range of tower thickness was identified. The maximum von Mises stresses and the horizontal sways of the tower plotted against T for the 50 m-towers are presented in Figure 11.
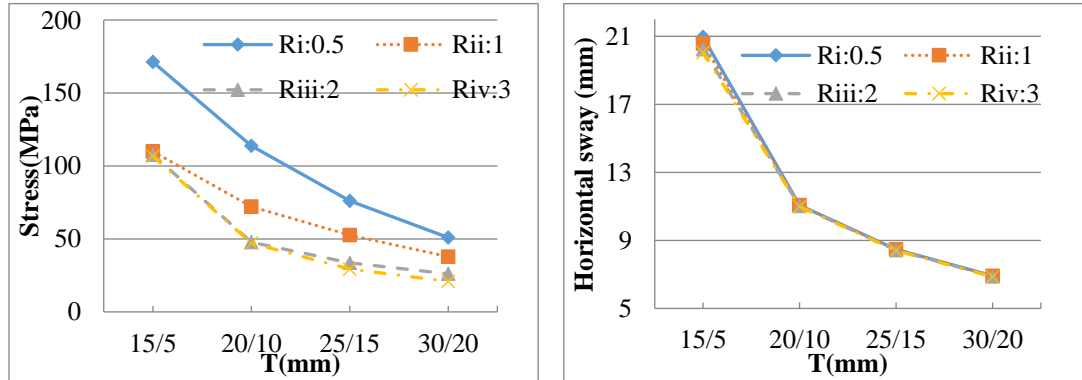

Figure 11. Maximum von Mises stress and horizontal sway versus T of the 50H_i.

The 50 m tower with a ring spacing of H_i is denoted as 50 H_i. In Figure 11 the horizontal axis represents the T of 50 H_i and the vertical axis corresponded to the maximum von Mises stresses or the horizontal sways of 50 H_i. Clearly, the maximum von Mises stress and the horizontal sway of the 50 m towers reduced as the thickness increased from T_i to T_{iv} in accordance with Figure 11 and Appendix A.

Furthermore, the rate of change of the maximum von Mises stress and of the horizontal sway of the 50 m-towers with respect to T were investigated in order to obtain the efficiency repowering range of thickness, based on its effect on the maximum von Mises stress and the sway of the towers. Where there is a high rate of change of the maximum von Mises stress and of the horizontal sway of the towers with respect to T, this indicates the significant range. The rate of change of the maximum von Mises stress and of the horizontal sway are given by the following general equations:

$$\frac{\Delta S}{\Delta T} = \begin{cases} (S_{Ti}-S_{Tii})/(T_{ii}-T_i) \\ (S_{Tii}-S_{Tiii})/(T_{iii}-T_{ii}) \\ (S_{Tiii}-S_{Tiv})/(T_{iv}-T_{iii}) \end{cases} \quad (2)$$

$$\frac{\Delta D}{\Delta T} = \begin{cases} (D_{Ti}-D_{Tii})/(T_{ii}-T_i) \\ (D_{Tii}-D_{Tiii})/(T_{iii}-T_{ii}) \\ (D_{Tiii}-D_{Tiv})/(T_{iv}-T_{iii}) \end{cases} \quad (3)$$

where the $\Delta S/\Delta T$ and $\Delta D/\Delta T$ respectively represent the rate of change of the maximum von Mises stress and of the horizontal sway of the wind tower with respect to T. S_{Ti}, S_{Tii}, S_{Tiii} and S_{Tiv} refer to the maximum von Mises stress of the 50 m-towers for each R and H. D_{Ti}, D_{Tii}, D_{Tiii} and D_{Tiv} refer to the maximum horizontal sway of the 50 m towers under the four specified values of R and H. Therefore, the $\Delta S/\Delta T$ and $\Delta D/\Delta T$ of the 50/150/250 H_i towers can be obtained by using Appendix A and Equations (2) and (3). In addition, the rate of change for the maximum von Mises stress and for the horizontal sway of the towers with different sizes and spacings of the stiffening rings can also be calculated substituting the results from Appendix A into Equations (2) and (3).

The rate of change of the maximum von Mises stress and of the horizontal sway of the 50 m-towers are presented in Figures 12–15. In general, the rate of change of the maximum von Mises stress and of the horizontal sway of the 50 m towers for each R and H reduced as T increased from T_i to T_{iv}. For the maximum horizontal sway, the rate of change of the 50 m-towers was very close for each T variation, which was 0.5 (T_i to T_{ii}), 0.14 (T_{ii} to T_{iii}) and 0.08 (T_{iii} to T_{iv}). For the maximum von Mises stress, the rate of change for the 50 m-towers as T increased from T_i to T_{ii}, were relatively greater than

those when T increased from T_{ii} to T_{iv} (as shown in Figures 12–15). The most critical repowering range of the shell wall thickness of the 50 m towers based on the changing rate was from T_i to T_{ii}. For the 150 m and 250 m-towers, the rate of change of the 150 m and 250 m-towers when T varied from T_i to T_{ii} were also greater than those of the 150 m and 250 m towers when T increased from T_{ii} to T_{iv}. The rate of change of the maximum horizontal sway of the 150 m and 250 m-towers in each T variation range were also fairly close. Compared with the three height cases, the rate of change of maximum horizontal sway tended to be linear curves with respect to each T variation for intermediate and high height towers. The efficiency repowering range of thickness variation in low height and thin walled towers was more critical than that in towers of greater height and in thick walled towers.
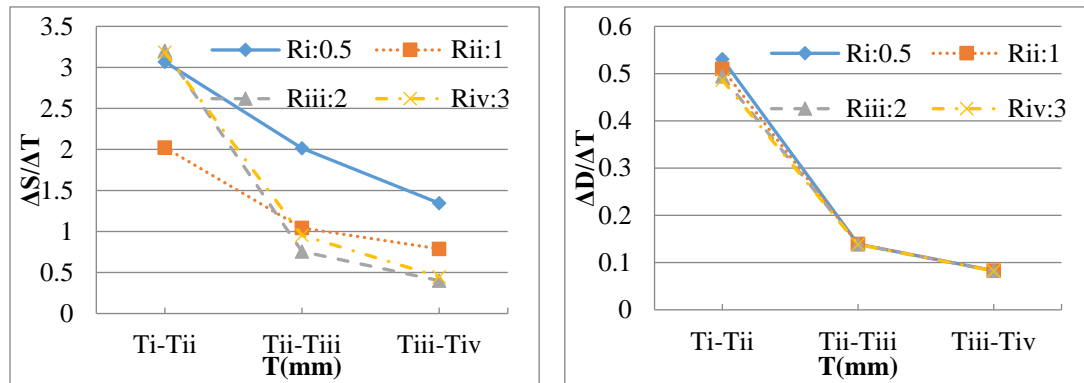

Figure 12. $\Delta S/\Delta T$ and $\Delta D/\Delta T$ of the $50H_i$ with respect to T.
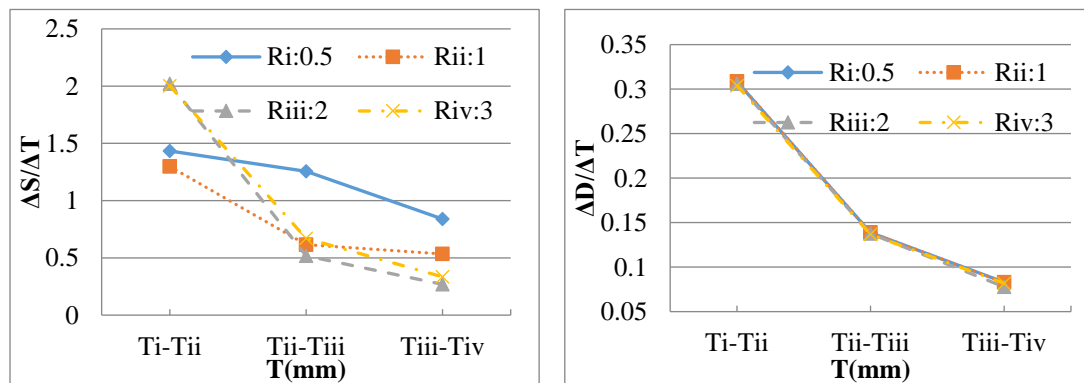

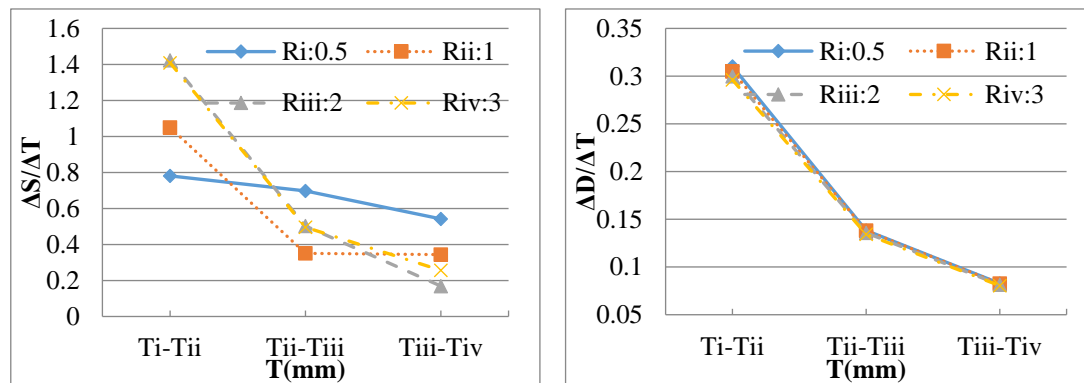**Figure 13.** $\Delta S/\Delta T$ and $\Delta D/\Delta T$ of the $50H_{ii}$ with respect to T.

Figure 14. $\Delta S/\Delta T$ and $\Delta D/\Delta T$ of the $50H_{iii}$ with respect to T.
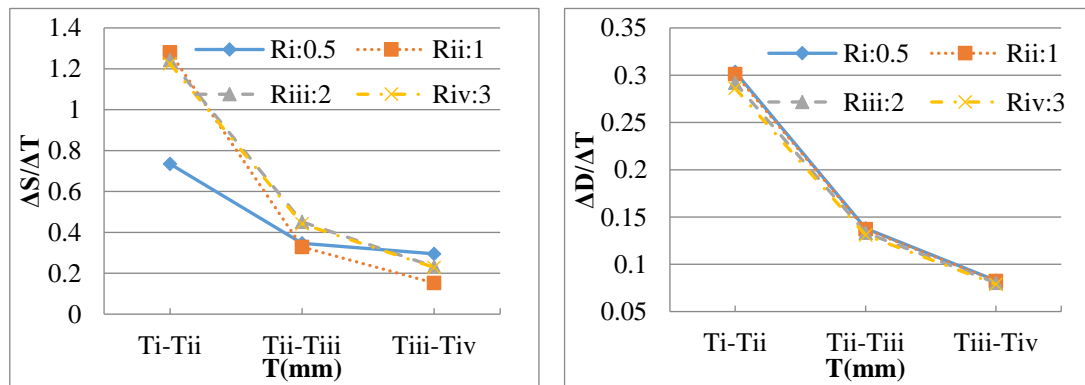
Figure 15. $\Delta S/\Delta T$ and $\Delta D/\Delta T$ of the $50H_{iv}$ with respect to T.

3.2.2. Efficiency Repowering Range of the Mid-Section Width-to-Thickness Ratio R of the Stiffening Rings

To resist local buckling, stiffening rings were added to the inner side of the towers. The mid-section width-to-thickness ratio of the rings, referred to as R, for the three height cases were 0.5, 1, 2 and 3 respectively. As the R_i, R_{ii}, R_{iii} and R_{iv} were taken at the same level in the towers for each T and H, the maximum von Mises stresses in the towers could be compared.

The maximum von Mises stresses and horizontal sways versus R for the 50 H_i tower are shown in Figure 16. The horizontal axis represents the R of the 50 m-tower, and the vertical axis refers to the maximum von Mises stress and horizontal sway (Figure 16). For the 50 H_i, the maximum von Mises stresses and horizontal sways decreased as R increased. From Appendix A, it is concluded that the maximum von Mises stresses and horizontal sways of the 50 m, 150 m and 250 m towers were negative with reference to R.
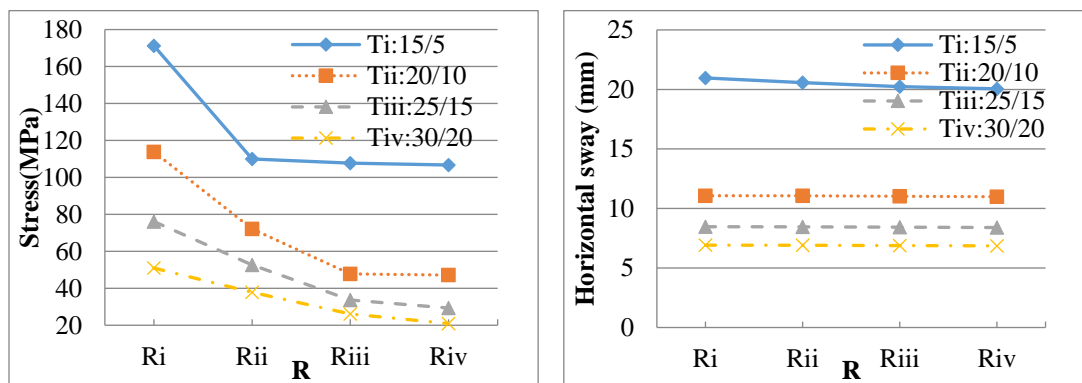

Figure 16. Maximum von Mises stresses and horizontal sways versus R of the 50 H_i.

The rate of change of the maximum von Mises stresses and of the horizontal sways of the 50 m, 150 m and 250 m towers with respect to R were also studied. The rate of change of the maximum von Mises stresses and of the horizontal sways with respect to R were higher in some ranges, indicating that the variations of maximum von Mises stress and horizontal sway lie in a more critical repowering range in affecting the strength of the towers with respect to R variation. The rate of change of the maximum von Mises stress and of the horizontal sway were obtained by the following general equations:

$$\frac{\Delta S}{\Delta R} = \begin{cases} (S_{Ri} - S_{Rii})/(R_{ii} - R_i) \\ (S_{Rii} - S_{Riii})/(R_{iii} - R_{ii}) \\ (S_{Riii} - S_{Riv})/(R_{iv} - R_{iii}) \end{cases} \tag{4}$$

$$\frac{\Delta D}{\Delta R} = \begin{cases} (D_{Ri}-D_{Rii})/(R_{ii}-R_{i}) \\ (D_{Rii}-D_{Riii})/(R_{iii}-R_{ii}) \\ (D_{Riii}-D_{Riv})/(R_{iv}-R_{iii}) \end{cases} \tag{5}$$

where the $\Delta S/\Delta R$ and $\Delta D/\Delta R$ refer to the rate of change of the maximum von Mises stresses and of the horizontal sways of the 50 m, 150 m and 250 m-towers with respect to R. S_{Ri}, S_{Rii}, S_{Riii} and S_{Riv} represent the maximum von Mises stresses of the tower structures for each H and T. D_{Ri}, D_{Rii}, D_{Riii} and D_{Riv} were the maximum horizontal sways of the 50 m, 150 m and 250 m towers for each H and T. Using Equations (4) and (5) and Appendix A, the $\Delta S/\Delta R$ and $\Delta D/\Delta R$ of the 50 m, 150 m and 250 m towers were calculated.

The rate of change of the maximum von Mises stress and of the horizontal sway of the 50/150/250 H_i towers are shown in Figures 17–19. The rate of change of the maximum von Mises stress of the 50/150/250H_i towers reduced consistently as R increased, as shown in Figures 17–19. The effect of variations in R on the maximum von Mises stress was far more significant than the effect on the maximum horizontal sway for each height case. For all three heights of tower, the rate of change when R increased from R_i to R_{ii} were greater than those when R increased from R_{ii} to R_{iv}, which indicates that R was more significant for the strength enhancement of towers when it was within the repowering range of a small ratio (e.g., 0.5 to 1). Furthermore, the effect of variations in R on strength enhancement for low and intermediate towers was greater than that for high towers because the $\Delta S/\Delta R$ of the 50 m and 150 m towers were greater than those of the 250 m towers.
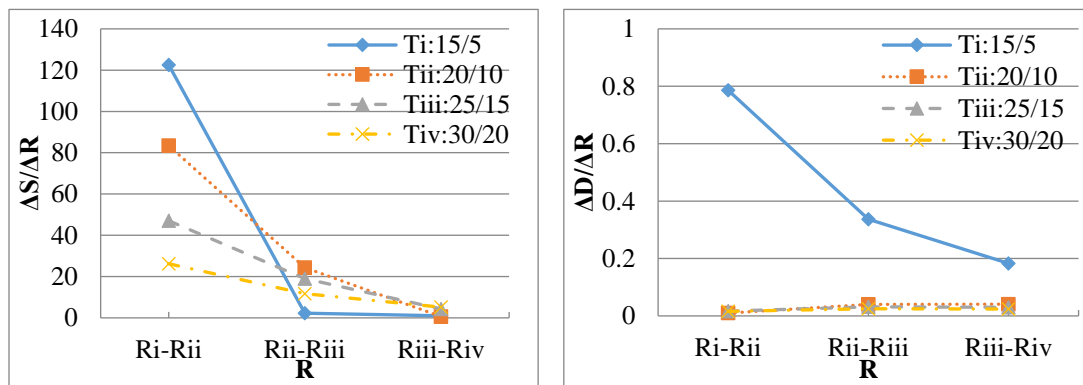
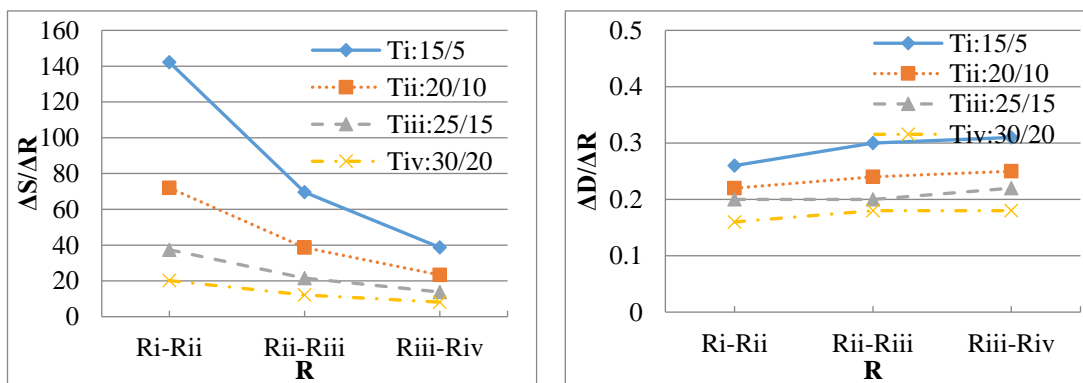**Figure 17.** $\Delta S/\Delta R$ and $\Delta D/\Delta R$ of the 50H_i with respect to R.

Figure 18. $\Delta S/\Delta R$ and $\Delta D/\Delta R$ of the 150H_i with respect to R.
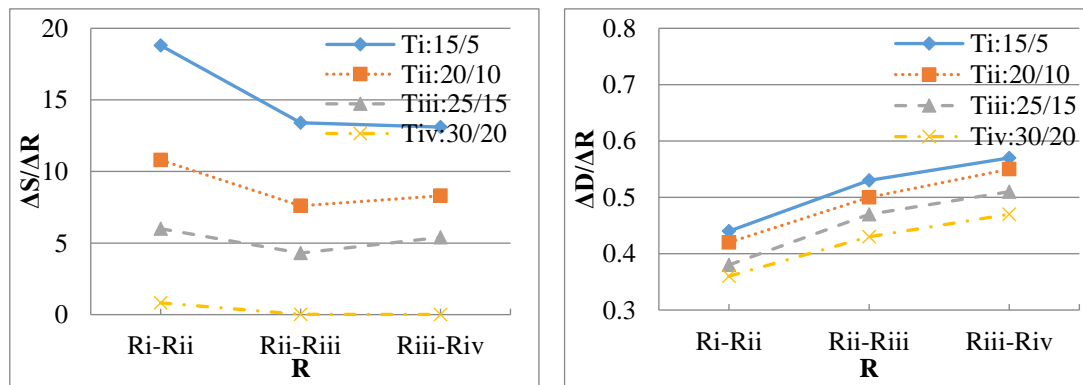
Figure 19. $\Delta S/\Delta R$ and $\Delta D/\Delta R$ of the $250H_i$ with respect to R.

3.2.3. Efficiency Repowering Range of the Spacing H

Stiffening rings are designed and manufactured to strengthen the tower against shell buckling. For these rings, an appropriately chosen distance between two neighboring stiffening rings should be investigated for each height case. For each T and R, the maximum von Mises stresses in the shell of the towers were compared.

The 50 m tower with thickness T_i was referred to as $50T_i$. The maximum von Mises stresses and the horizontal sways versus H for the 50 m tower with T_i are presented in Figure 20. At the horizontal axis, the H of the 50 m-tower, and at the vertical axis the maximum von Mises stresses or the horizontal sways of each tower is depicted (Figure 20). Clearly, the maximum von Mises stresses and the horizontal sways reduced as H decreased, as can be seen in Appendix A. The rate of change of the maximum von Mises stress and of the horizontal sway of $50/150/250T_i$ with respect to H can be obtained by referring to Equations (6) and (7) and Appendix A. The greater the $\Delta S/\Delta H$ and $\Delta D/\Delta H$ of the towers, the more critical is the variation of the spacing, H, in the strengthening of the tower. The general equations:

$$\frac{\Delta S}{\Delta H} = \left\{ \begin{array}{l} (S_i - S_{ii})/(H_{ii} - H_i) \\ (S_{ii} - S_{iii})/(H_{iii} - H_{ii}) \\ (S_{iii} - S_{iv})/(H_{iv} - H_{iii}) \end{array} \right. \tag{6}$$

$$\frac{\Delta D}{\Delta H} = \left\{ \begin{array}{l} (D_i - D_{ii})/(H_{ii} - H_i) \\ (D_{ii} - D_{iii})/(H_{iii} - H_{ii}) \\ (D_{iii} - D_{iv})/(H_{iv} - H_{iii}) \end{array} \right. \tag{7}$$

were introduced, where the $\Delta S/\Delta H$ and $\Delta D/\Delta H$ represent the rate of change of the maximum von Mises stresses and of the horizontal sways of the towers respectively. S_i, S_{ii}, S_{iii} and S_{iv} are the maximum von Mises stresses of the towers. D_i, D_{ii}, D_{iii} and D_{iv} refer to the maximum horizontal sways of the towers, and H_i, H_{ii}, H_{iii} and H_{iv} are the four distances between neighboring rings at each of the towers of height 50 m, 150 m and 250 m.
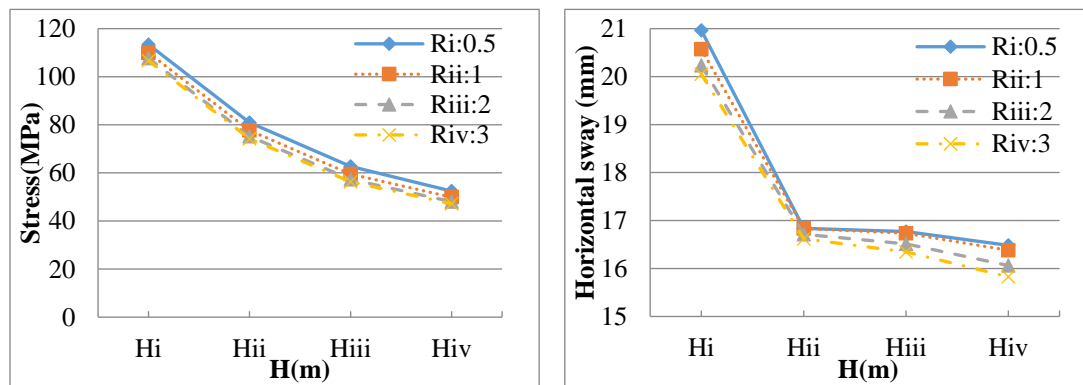
Figure 20. Maximum von Mises stresses and horizontal sways versus H of $50T_i$.

The rate of change of the maximum von Mises stresses and of the horizontal sways of the $50T_i/T_{ii}/T_{iii}/T_{iv}$ towers with respect to H are displayed in Figures 21–24. For the 50 m towers, the effect of varying H on the rate of change of the maximum von Mises stresses was more significant than the effect on the rate of change of the maximum horizontal sway. The rate of change of the maximum von Mises stresses of the $50T_i$ tower with respect to H varied slightly (with a range of approximately 4.4–4.9) as shown in Figure 21. However, the rate of change of the maximum horizontal sways of the $50T_i$ tower with H varying from H_i to H_{ii} were greater than those when H increased from H_{ii} to H_{iv}. Thus, the more significant repowering range in H variation for $50T_i$ was from H_i to H_{ii}. However, for $50T_{ii}/T_{iii}/T_{iv}$, the repowering range from H_{iii} to H_{iv} was the most significant one when strengthening the 50 m towers by decreasing rings spacing, as indicated in Figures 22–24. For thin walled towers, a greater gap between two neighboring rings is a better option for strength enhancement, whereas for intermediate and thick walled towers, the effective repowering range for enhancing tower strength was where the neighboring rings were spaced at shorter intervals.
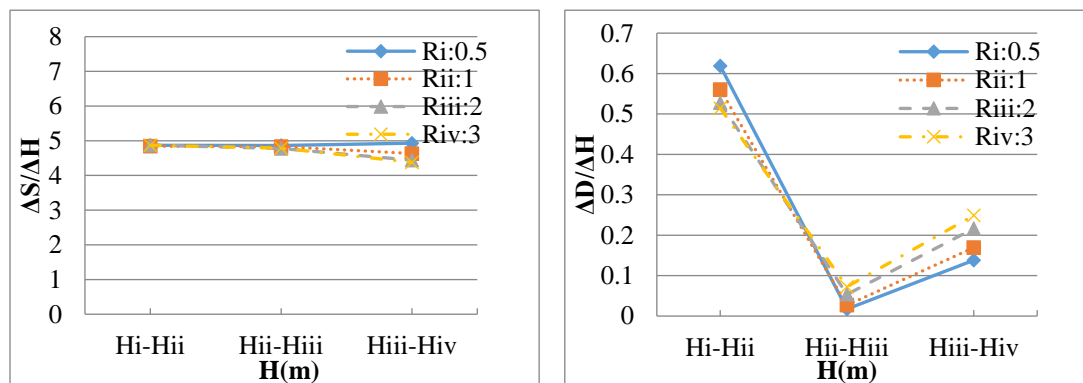

Figure 21. $\Delta S/\Delta H$ and $\Delta D/\Delta H$ graphs of the $50T_i$ with respect to H.
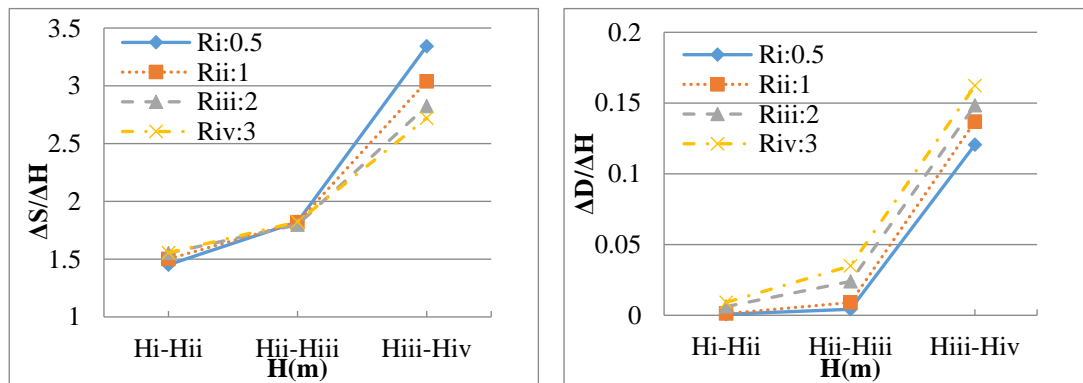
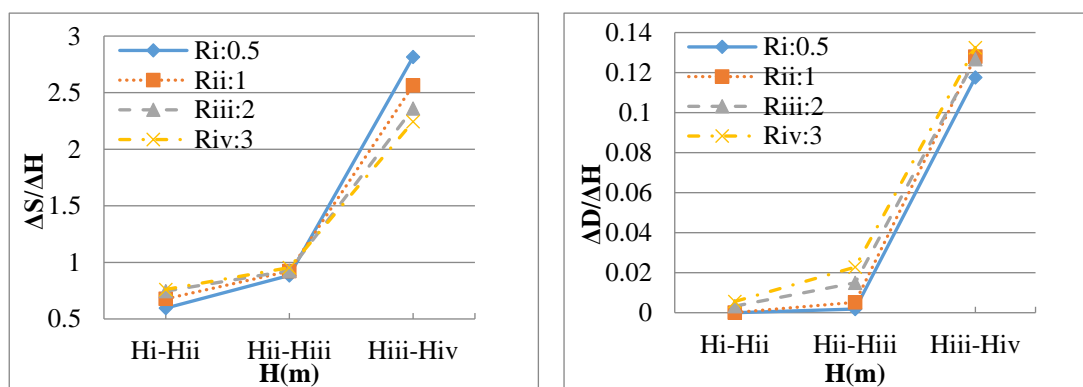**Figure 22.** $\Delta S/\Delta H$ and $\Delta D/\Delta H$ graphs of the $50T_{ii}$ with respect to H.

Figure 23. $\Delta S/\Delta H$ and $\Delta D/\Delta H$ graphs of the $50T_{iii}$ with respect to H.
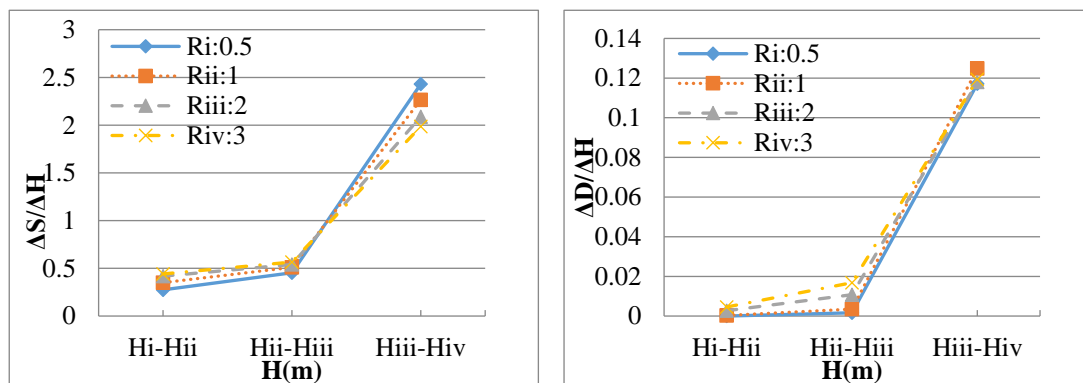

Figure 24. $\Delta S/\Delta H$ and $\Delta D/\Delta H$ graphs of the $50T_{iv}$ with respect to H.

For the 150 m-towers, the rate of change of the maximum von Mises stresses and of the horizontal sways of the $150T_i$ due to H variation are presented in Figure 25. As the peak of rate of change of the maximum von Mises stress and of the horizontal sway lay in the range of H_{ii} to H_{iii}, the most significant repowering range of H variation for the 150 m towers was from H_{ii} to H_{iii}. Concerning the 250 m-towers, Figure 26 shows the rate of change of the maximum von Mises stresses and of the horizontal sways of the $250T_i$ tower with respect to H. Clearly, H varying from H_i to H_{ii} was the most significant repowering range with respect to the strengthening of the towers. Concerning intermediate and high towers, the most significant repowering ranges of two neighboring rings were respectively the intermediate distance and the long spans.
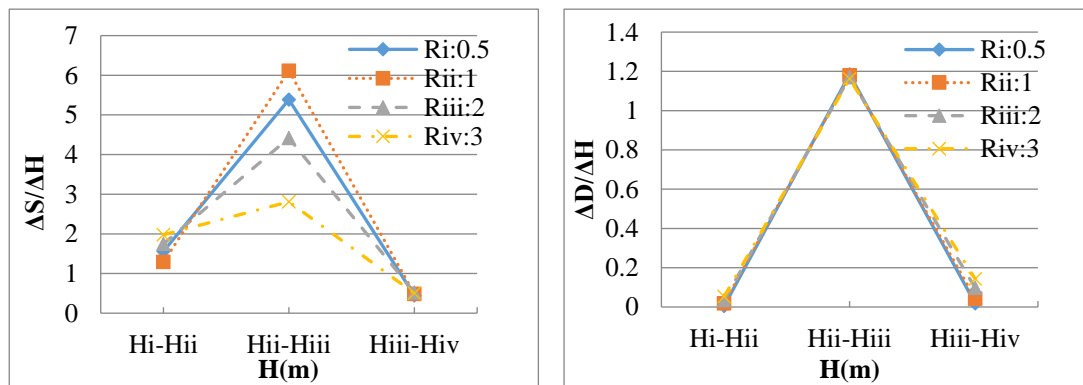
Figure 25. ΔS/ΔH and ΔD/ΔH graphs of the $150T_i$ with respect to H.
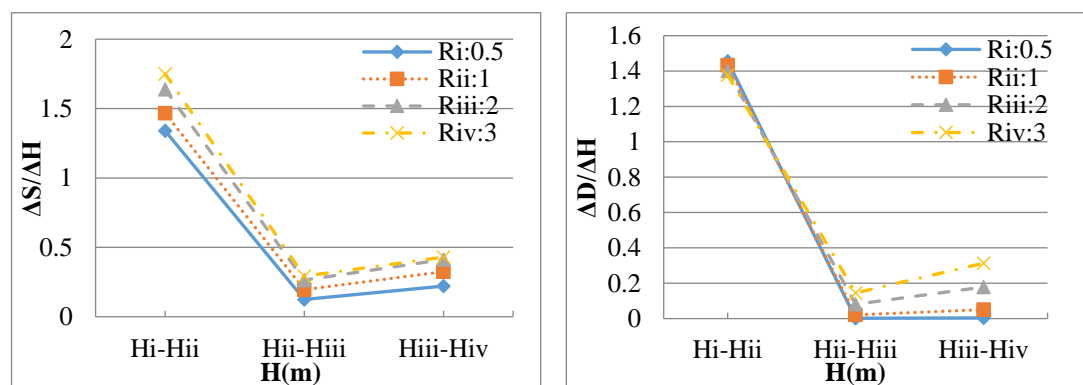
Figure 26. ΔS/ΔH and ΔD/ΔH graphs of the $250T_i$ with respect to H.

4. Conclusions

In this study, the aim was to propose the efficiency repowering range of design variables so that the repowering of the wind turbine system can be performed more efficiently. Firstly, an effective numerical model was validated against experimental data. In addition, a sensitivity analysis of the finite element models used was performed so that the optimum element size can be defined. The simulated maximum stresses of the monitored towers were fairly close to the measured ones in the instrumented tower at the same heights. Furthermore, the maximum horizontal sways measured by the sensors were fairly close to the maximum horizontal displacements modeled using a numerical simulation method. Thus, the numerical simulation method appeared to be sufficiently effective to simulate the structural response of tubular steel wind turbine towers.

With reference to the efficiency repowering range of design variables, the tower shell thickness T, the width-to-thickness ratio R and the ring spacing H were considered as design variables for each tower height case. For all three tower heights, the strengthening effect on the towers was positive with reference to the variations of wall thickness and the ratio of width-to-thickness. In particular, the more significant repowering range of wall thickness, T, for strength enhancement of the towers was at the thin walled category (e.g., T_i to T_{ii}). For the ratios R, the change of the strength of the towers was most important at the small ratio category (e.g., R_i to R_{ii}). Therefore, the efficiency repowering range of the towers for the wall thickness and the ratio of width-to-thickness were respectively the small ratio category. Concerning the ring spacing, the efficiency repowering range for the low height level tower with a thin walled thickness was at the greater height (e.g., H_i to H_{ii}), but with an intermediate and thick wall thickness, the efficiency repowering range at the category of lower height (e.g., H_{iii} to H_{iv}) was a better option in cost saving for the strengthening of the towers. Furthermore, the efficiency repowering range for ring spacing for the intermediate and high height towers for increasing tower

strength was at the level of intermediate distance and long distance respectively (e.g., H_{ii} to H_{iii} and H_i to H_{ii}).

Appendix A

Table A1. Maximum von Mises stresses and horizontal sways of the 50 m, 150 m and 250 m-towers.

Types of Towers	Max. Stress (MPa)			Max. Stress of Shell (MPa)			Max. Horizontal Sway (mm)		
	50 m	150 m	250 m	50 m	150 m	250 m	50 m	150 m	250 m
$T_iR_iH_i$	171.2	351.2	208.9	113.4	91.14	107.6	20.96	199.4	648.75
$T_{ii}R_iH_i$	113.8	230.4	152.9	50.89	65.94	98.74	11.07	176.15	598.28
$T_{iii}R_iH_i$	76.1	154.9	113.7	31.30	57.17	91.45	8.47	157.8	555.10
$T_{iv}R_iH_i$	50.94	106.8	85.79	21.88	51.62	85.39	6.92	143.05	517.76
$T_iR_{ii}H_i$	109.9	280.1	199.5	109.9	89.96	107.47	20.57	199.27	648.53
$T_{ii}R_{ii}H_i$	72.09	194.4	147.5	49.1	64.75	98.65	11.07	176.04	598.07
$T_{iii}R_{ii}H_i$	52.58	136.2	110.7	30.47	56.91	91.42	8.46	157.75	554.91
$T_{iv}R_{ii}H_i$	37.84	96.71	85.379	21.53	51.49	85.38	6.91	142.97	517.58
$T_iR_{iii}H_i$	107.7	210.5	186.1	107.7	83.08	107.2	20.23	198.97	648.00
$T_{ii}R_{iii}H_i$	47.75	155.8	139.9	47.75	63.02	98.50	11.03	175.8	597.57
$T_{iii}R_{iii}H_i$	33.61	114.7	106.4	29.70	56.47	91.35	8.43	157.55	554.44
$T_{iv}R_{iii}H_i$	26.11	84.59	85.36	21.15	51.26	85.36	6.88	142.79	517.15
$T_iR_{iv}H_i$	106.7	171.8	173.0	106.7	76.84	106.9	20.05	198.66	647.43
$T_{ii}R_{iv}H_i$	47.14	132.5	131.6	47.14	62.37	98.35	10.99	175.55	597.02
$T_{iii}R_{iv}H_i$	29.31	100.9	101.0	29.31	56.11	91.29	8.40	157.33	553.93
$T_{iv}R_{iv}H_i$	20.92	76.45	85.35	20.92	51.07	85.35	6.86	142.61	516.68
$T_iR_iH_{ii}$	110.7	327.7	308.2	80.93	85.28	96.47	16.84	199.38	636.62
$T_{ii}R_iH_{ii}$	83.88	221.1	243.5	41.21	64.20	88.36	11.07	176.13	586.11
$T_{iii}R_iH_{ii}$	60.39	151.6	195.7	27.33	57.09	81.64	8.47	157.82	542.93
$T_{iv}R_iH_{ii}$	44.68	106.2	159.8	20.05	51.58	76.0	6.92	143.03	505.6
$T_iR_{ii}H_{ii}$	77.65	272.1	266.8	77.65	85.12	95.25	16.84	199.2	636.59
$T_{ii}R_{ii}H_{ii}$	53.36	195.5	215.4	39.09	63.56	87.50	11.06	175.98	585.99
$T_{iii}R_{ii}H_{ii}$	41.83	140.2	175.9	25.95	56.76	81.02	8.46	157.7	542.77
$T_{iv}R_{ii}H_{ii}$	31.83	101.3	145.3	19.2	51.41	75.55	6.91	142.92	505.42
$T_iR_{iii}H_{ii}$	75.2	187.3	211.5	75.20	76.53	93.51	16.71	198.84	636.33
$T_{ii}R_{iii}H_{ii}$	37.4	143.6	175.1	37.4	62.58	86.23	10.99	175.67	585.64
$T_{iii}R_{iii}H_{ii}$	27.71	109.2	146.1	24.73	56.23	80.09	8.41	157.44	542.38
$T_{iv}R_{iii}H_{ii}$	22.68	82.66	123.2	18.36	51.13	74.85	6.87	142.69	505.02
$T_iR_{iv}H_{ii}$	74.24	154.9	176.6	74.24	69.43	92.3	16.62	198.46	635.95
$T_{ii}R_{iv}H_{ii}$	36.77	122.5	148.5	36.77	61.82	85.33	10.92	175.36	585.23
$T_{iii}R_{iv}H_{ii}$	24.24	95.18	125.9	24.24	55.8	79.41	8.36	157.17	541.96
$T_{iv}R_{iv}H_{ii}$	17.98	73.28	107.5	17.98	50.89	74.33	6.83	142.46	504.61
$T_iR_iH_{iii}$	78.00	306.9	290.6	62.69	66.65	95.81	16.77	195.28	636.61
$T_{ii}R_iH_{iii}$	63.39	230.4	232.7	34.37	58.26	87.9	11.05	172.09	586.07
$T_{iii}R_iH_{iii}$	50.34	175.0	188.8	24.01	51.83	81.32	8.46	153.83	542.87
$T_{iv}R_iH_{iii}$	40.2	134.7	155.1	18.35	46.73	75.76	6.91	139.07	505.52
$T_iR_{ii}H_{iii}$	59.53	214.9	241.4	59.53	63.97	94.21	16.73	195.12	636.48
$T_{ii}R_{ii}H_{iii}$	39.9	169.8	197.8	32.27	56.54	86.76	11.02	171.94	585.82
$T_{iii}R_{ii}H_{iii}$	33.34	134.8	163.5	22.49	50.66	80.49	8.44	153.69	542.58
$T_{iv}R_{ii}H_{iii}$	26.91	107.7	136.3	17.29	45.92	75.15	6.89	138.94	505.22
$T_iR_{iii}H_{iii}$	57.29	137.0	185.6	57.29	61.25	92.11	16.51	194.79	635.9

Table A1. *Cont.*

Types of Towers	Max. Stress (MPa)			Max. Stress of Shell (MPa)			Max. Horizontal Sway (mm)		
	50 m	150 m	250 m	50 m	150 m	250 m	50 m	150 m	250 m
$T_{ii}R_{iii}H_{iii}$	30.66	113.0	156.3	30.66	54.59	85.19	10.90	171.64	585.18
$T_{iii}R_{iii}H_{iii}$	21.25	93.31	132.5	21.25	49.25	79.31	8.35	153.42	541.92
$T_{iv}R_{iii}H_{iii}$	18.09	77.38	112.9	16.34	44.89	74.26	6.83	138.7	504.56
$T_{i}R_{iv}H_{iii}$	56.29	101.4	147.7	56.29	59.71	90.75	16.35	194.44	635.18
$T_{ii}R_{iv}H_{iii}$	29.93	85.35	126.6	29.93	53.44	84.15	10.79	171.34	584.46
$T_{iii}R_{iv}H_{iii}$	20.66	71.96	109.0	20.66	48.39	78.50	8.28	153.16	541.21
$T_{iv}R_{iv}H_{iii}$	15.86	60.83	94.25	15.86	44.24	73.64	6.77	138.47	503.9
$T_{i}R_{i}H_{iv}$	52.42	274.9	279.5	52.42	65.68	95.20	16.48	195.24	636.6
$T_{ii}R_{i}H_{iv}$	38.68	211.1	225.0	27.41	57.71	87.47	10.80	172.05	586.00
$T_{iii}R_{i}H_{iv}$	32.20	163.3	183.4	18.15	51.46	81.01	8.22	153.79	542.77
$T_{iv}R_{i}H_{iv}$	26.68	127.6	151.1	13.29	46.48	75.54	6.67	139.04	505.43
$T_{i}R_{ii}H_{iv}$	49.88	188.0	224.0	49.88	62.92	93.32	16.38	195.03	636.34
$T_{ii}R_{ii}H_{iv}$	25.94	151.6	186.0	25.94	55.81	86.11	10.74	171.85	585.64
$T_{iii}R_{ii}H_{iv}$	19.79	122.6	155.6	17.15	50.15	80.01	8.17	153.62	542.38
$T_{iv}R_{ii}H_{iv}$	16.94	99.54	131.1	12.57	45.56	74.79	6.63	138.88	505.02
$T_{i}R_{iii}H_{iv}$	48.04	114.5	159.3	48.04	60.13	90.98	16.06	194.58	635.41
$T_{ii}R_{iii}H_{iv}$	24.78	96.26	136.4	24.78	53.77	84.34	10.59	171.46	584.68
$T_{iii}R_{iii}H_{iv}$	16.34	80.96	117.2	16.34	48.64	78.66	8.09	153.27	541.43
$T_{iv}R_{iii}H_{iv}$	11.99	68.47	101.2	11.99	44.44	73.76	6.58	138.56	504.1
$T_{i}R_{iv}H_{iv}$	47.17	86.74	128.1	47.17	58.63	89.57	15.83	194.13	634.32
$T_{ii}R_{iv}H_{iv}$	24.26	74.4	111.2	24.26	52.63	83.23	10.46	171.07	583.64
$T_{iii}R_{iv}H_{iv}$	15.99	63.89	96.80	15.99	47.77	77.8	8.0	152.92	540.44
$T_{iv}R_{iv}H_{iv}$	11.72	54.96	84.56	11.72	43.78	73.09	6.52	138.26	503.17

References

1. Martíneza, E.; Latorre-Bielb, J.I.; Jiménezc, E.; Sanza, F.; Blancoa, J. Life cycle assessment of a wind farm repowering process. *Renew. Sustain. Energy Rev.* **2018**, *93*, 260–271. [CrossRef]
2. Buchsbaum, L.; Patel, S. Wind turbine repowering is on the horizon. *Power* **2016**, *160*, 52–55.
3. Tziavos, N.; Hemida, H.; Metje, N.; Baniotopoulos, C. Non-linear Finite Element Analysis of Grouted Connections for Offshore Monopile Wind Turbines. *Ocean Eng.* **2018**, *171*, 633–645. [CrossRef]
4. Tziavos, N.I.; Hemida, H.; Dirar, S.; Papaelias, M.; Metje, N.; Baniotopoulos, C.C. Structural health monitoring of grouted connections for offshore wind turbines by means of acoustic emission: An experimental study. *Renew. Energy* **2019**, *147*, 130–140. [CrossRef]
5. Li, Z.-Q.; Chen, S.-J.; Ma, H.; Feng, T. Design defect of wind turbine operating in typhoon activity zone. *Eng. Fail. Anal.* **2013**, *27*, 165–172. [CrossRef]
6. Kilic, G.; Unluturk, M.S. Testing of wind turbine towers using wireless sensor network and accelerometer. *Renew. Energy* **2015**, *75*, 318–325. [CrossRef]
7. Binh, L.V.; Ishihara, T.; Phuc, P.V.; Fujino, Y. A peak factor for non-Gaussian response analysis of wind turbine tower. *J. Wind Eng. Ind. Aerodyn.* **2008**, *96*, 2217–2227. [CrossRef]
8. Kim, D.H.; Lee, S.G.; Lee, I.K. Seismic fragility analysis of 5 MW offshore wind turbine. *Renew. Energy* **2014**, *65*, 250–256. [CrossRef]
9. Tondini, N.; Hoang, V.L.; Demonceau, J.F.; Franssen, J.M. Experimental and numerical investigation of high-strength steel circular columns subjected to fire. *J. Constr. Steel Res.* **2013**, *80*, 57–81. [CrossRef]
10. Van der Woude, C.; Narasimhan, S. A study on vibration isolation for wind turbine structures. *Eng. Struct.* **2014**, *60*, 223–234. [CrossRef]
11. Tran, A.T.; Veljkovic, M.; Rebelo, C.; Simões da Silva, L. Resistance of door openings in towers for wind turbines. In Proceedings of the Third South-East European Conference on Computational Mechanics 2013, Kos Island, Greece, 12–14 June 2013.
12. Do, T.Q.; Mahmoud, H.; van de Lindt, J.W. Fatigue life of wind turbine tower bases throughout Colorado. *J. Perfor. Constr. Facil.* **2014**, *29*, 04014109. [CrossRef]

13. Schneider, W.; Zahlten, W. Load-bearing behaviour and structural analysis of slender ring-stiffened cylindrical shells under quasi-static wind load. *J. Constr. Steel Res.* **2004**, *60*, 125–146. [CrossRef]

14. Valamanesh, V.; Myers, A.T. Aerodynamic Damping and Seismic Response of Horizontal Axis Wind Turbine Towers. *J. Struct. Eng.* **2014**, *140*, 04014090. [CrossRef]

15. Guo, L.; Yang, S.; Jiao, H. Behavior of thin-walled circular hollow section tubes subjected to bending. *Thin-Walled Struct.* **2013**, *73*, 281–289. [CrossRef]

16. Ghanbari Ghazijahani, T.; Jiao, H.; Holloway, D. Structural behavior of shells with different cutouts under compression: An experimental study. *J. Constr. Steel Res.* **2015**, *105*, 129–137. [CrossRef]

17. Sabouri-Ghomi, S.; Kharrazi, M.H.K.; Javidan, P. Effect of stiffening rings on buckling stability of R.C. hyperbolic cooling towers. *Thin-Walled Struct.* **2006**, *44*, 152–158. [CrossRef]

18. Perelmuter, A.; Yurchenko, V. Parametric optimization of steel towers of high-power wind turbines. 11th international conference on modern building materials, structures and techniques, MBMST. *Procedia Eng.* **2013**, *57*, 895–905. [CrossRef]

19. Sim, H.-B.; Prowell, I.; Elgamal, A.; Uang, C.-M. Flexural tests and associated study of a full-scale 65-kW wind turbine tower. *J. Struct. Eng.* **2014**, *140*, 04013110. [CrossRef]

20. Hu, Y.; Baniotopoulos, C.C.; Yang, J. Effect of internal stiffening rings and wall thickness on the structural response of steel wind turbine towers. *Eng. Struct.* **2014**, *81*, 148–161. [CrossRef]

21. Negm, H.M.; Maalawi, K.Y. Structural design optimization of wind turbine towers. *Comput. Struct.* **2000**, *74*, 649–666. [CrossRef]

22. Shi, G.; Jiang, X.; Zhou, W.; Chan, T.-M.; Zhang, Y. Experimental study on column buckling of 420MPa high strength steel welded circular tubes. *J. Constr. Steel Res.* **2014**, *100*, 71–81. [CrossRef]

23. Zhu, J.H.; Young, B. Design of cold-formed steel oval hollow section columns. *J. Constr. Steel Res.* **2012**, *71*, 26–37. [CrossRef]

24. Karpat, F. A virtual tool for minimum cost design of a wind turbine tower with ring stiffeners. *Energies* **2013**, *6*, 3822–3840. [CrossRef]

25. Chen, J.; Xu, Y.; Li, J. Numerical investigation of the strengthening method by circumferential prestressing to improve the fatigue life of embedded-ring concrete foundation for onshore wind turbine tower. *Energies* **2020**, *13*, 533. [CrossRef]

26. Ding, H.; Feng, Z.; Zhang, P.; Le, C.; Guo, Y. Floating performance of a composite bucket foundation with an offshore wind tower during transportation. *Energies* **2020**, *13*, 882. [CrossRef]

27. ABAQUS/Standard and ABAQUS/Explicit-Version 6.8-1. In *Abaqus Theory Manual, Dassault System*; Dassault System: Paris, France, 2008.

28. Rebelo, C.; Veljkovic, M.; Simões da Silva, L.; Simões, R.; Henriques, J. Structural monitoring of a wind turbine steel tower Part I system description and calibration. *Wind Struct.* **2012**, *15*, 285–299. [CrossRef]

29. Rebelo, C.; Veljkovic, M.; Matos, R.; Simões da Silva, L. Structural monitoring of a wind turbine steel tower Part II monitoring results. *Wind Struct.* **2012**, *15*, 301–311. [CrossRef]

30. *ENV 1991-01-04: Actions on Structures*; CEN: Brussels, Belgium, 1991.

31. Lavassas, I.; Nikolaidis, G.; Zervas, P.; Efthimiou, E.; Doudoumis, I.N.; Baniotopoulos, C.C. Analysis and design of the prototype of a steel 1-MW wind turbine tower. *Eng. Struct.* **2003**, *25*, 1097–1106. [CrossRef]

32. Baniotopoulos, C.C.; Borri, C.; Stathopoulos, T. (Eds.) *Environmental Wind Engineering and Design of Wind Energy Structures*; Springer: New York, NY, USA, 2010.